Visible and Near-infrared Photoluminescence Enhanced by Ag Nanoparticles in Sm^{3+}-doped Aluminoborate Glass

Yuan Gao[1], Shunsuke Murai[1*], Koji Fujita[1], and Katsuhisa Tanaka[1]

1. Department of Material Chemistry, Graduate School of Engineering, Kyoto University, Katsura, Nishikyo-ku, Kyoto 615-8510, Japan

Abstract: Sm^{3+}-doped aluminoborate glasses containing Ag nanoparticles have been synthesizeed via a melt-quenching technique. After heat treatment, the surface plasmon resonance (SPR) absorption peak of Ag nanoparticles appears approximately at the wavelength λ = 425 nm. With the precipitation of the Ag nanoparticles, the intensities of visible (λ = 600 nm) and near-infrared (λ = 950 nm) photoluminescence are enhanced under excitation at λ = 400 nm up to 39.8% and 25% that of the as-made glass, respectively. Moreover, the excitation of Sm^{3+} at λ = 473 nm for the sample heat-treated at 500 °C shows higher enhancement in near-infrared photoluminescence by 55.5% (λ = 950 nm). This enhancement is attributable to the intensified localized electromagnetic field accompanied by the excitation of SPR. The presence of Ag nanoparticles assists the conversion of UV light into visible and near-infrared light, which can induce a photoelectric effect for Si and other semiconductors used in solar cells.

Key Words: Ag nanoparticles, Downconversion photoluminescence, Surface plasmon resonance, Si solar cell.

* Corresponding author.

E-mail address: murai@dipole7.kuic.kyoto-u.ac.jp

1. Introduction

Solar energy is a free, ubiquitous, stable, and inexhaustible source of energy [1] and solar cells can convert solar energy into electrical energy without producing by-products. The power generation by solar cells is based on the photoelectric properties of certain materials [2-4]. Only when exposed to light with the wavelengths (λ) matched to the bandgap, pairs of holes and electrons are generated and an electric current is produced [5,6]. For example, the band gap for Si crystal, which is the most widely used material for solar cells, is approximately 1.155 eV at room temperature, and hence, solar light with $\lambda > 1100$ nm cannot be absorbed and is wasted. Moreover, under ultraviolet (UV) ($\lambda < 400$ nm) irradiation, the excess photon energy is converted into heat and wasted. One way to efficiently use the solar spectrum is to up-convert near-infrared light to light with $\lambda < 1100$ nm, which can be absorbed by Si [7,8]. The other way is down-conversion where light with shorter λ is converted into light with longer λ. Therefore, the application of up- and down-conversions can expand the response bandwidth of Si and other solar cell materials to the solar spectrum.

Rare-earth-doped ceramics and glasses are the most intensively investigated materials as solar spectral converters and have been combined with solar cells to improve the efficiency of light-to-electricity conversion [9-12]. In particular, inorganic glasses containing rare earth ions are promising owing to the combination of the high internal quantum yield of rare earth ions and the practical stability and formability of glass. The bottleneck is the low absorption of rare earth ions. Although they can convert absorbed light into luminescence efficiently, the absorption cross-section of rare earths is small, i.e. the external quantum yield is low, and hence, the conversion efficiency remains low.

It is well known that plasmonic metal nanostructures can focus the incoming light on their surfaces and enhance the local electric field by the excitation of surface plasmon resonance (SPR). The coupling of SPR and fluorescence materials resulting in an enhanced photoluminescence (PL) has been reported in rare-earth-doped glasses containing metallic nanoparticles [13-19]. Among the rare-earth ions, Sm^{3+} has a $4f^5$ electron configuration and shows strong PL in the orange-red (λ ~ 580–660 nm) and near-infrared regions (λ ~ 0.95–1.32 μm) under excitation at λ = 400 nm, which makes Sm^{3+}-doped glasses good candidates for solar spectral converters [20, 21]. Several researchers have focused on the PL enhancement owing to Sm^{3+} via SPR in various glass matrixes,

such as tellurite-based glass [22-25], phosphate-based glass [26,27], lead-based glass [28], oxyfluoride glass [29], antimony glass [30], chloroborosilicate glass [31], and ion-exchanged alkali containing glass [32,33]. Feras et al. enhanced the PL intensity of Sm^{3+} up to seven times in tellurite glass [22]. Karmakar et al. reported that, in chloroborosilicate glass doped with Ag nanoparticles, the PL of Sm^{3+} at λ = 600–650 nm was slightly enhanced by up to 4% [31]. Herrera et al. fabricated Sm^{3+}-doped B_2O_3-PbO-Bi_2O_3-GeO_2 glass containing Ag nanoparticles via Ag^+-K^+ ion exchange, and enhanced PL both in the visible (60%) and near-infrared (5%) regions [28]. Ag is mainly used for visible PL enhancement owing to its excellent plasmonic properties in the visible wavelength region. However, the analysis is rendered complex by the presence of optically active Ag-related species. Ag^+ clusters including Ag^+ dimer and trimer can absorb and emit light, which can conceal the plasmonic contribution to the PL enhancement. For example, Qiu et al. [32] and Thomas et al. [33] reported the influence of such molecule-like Ag clusters that act as an energy donor to Sm^{3+} to enhance the PL.

Aluminoborate glasses are highly homogeneous and stable glasses with low melting point. These glass matrixes allow homogeneous dispersion of an active centre and the precipitation of Ag nanoparticles [34] while avoiding the formation of Ag^+ clusters. Although aluminoborate glass is a suitable matrix to investigate the effect of Ag nanoparticles on the PL properties of a luminescence centre, there have not been many detailed studies in this regard. In the present study, we investigated the effect of SPR of Ag nanoparticles on the visible and near-infrared PL of Sm^{3+} in aluminoborate glasses. Compared with the as-made glass, the heat-treated glass samples showed SPR absorption peaks. Under excitation at λ = 400 nm, both 4f – 4f transitions of Sm^{3+} and SPR were induced simultaneously, which increased the intensity of visible and infrared PL through down-conversion of Sm^{3+} up to 39.8% (λ = 600 nm) and 25% (λ = 950 nm) in the visible and infrared regions, respectively. Under excitation at λ = 473 nm, three near-infrared PL peaks were significantly enhanced by 55.5% (λ = 950 nm), 50% (1193 nm), and 52% (1289 nm).

2. Experiment

The precursor glasses were prepared with the nominal composition of $65B_2O_3$-$27Na_2CO_3$-$8Al_2O_3$-$0.2Sm_2O_3$-$1AgNO_3$ (in mol%). Batches of 10 g of the starting materials were fully mixed and melted in a covered alumina crucible in air at 1400 °C for 40 min, and cast into a steel mould, followed by heat treatment at 350, 400, 450, 500, and 550 °C for 1 h.

The samples heat-treated thus will be referred to as HT350, HT400, HT450, HT500, and HT550, respectively.

The thermogravimetric and differential thermal analysis (TG-DTA, TG-8120, Rigaku, Japan) measurement was carried out from room temperature to 1000 °C at the rate of 10 $Kmin^{-1}$ in air. The microstructures of the samples were observed using a transmission electron microscope (TEM, JEM-2010, Japan). Optical absorption spectra were recorded in the range λ=200–1500 nm using a JASCO V-570 near-infrared–visible–ultraviolet (NIR–Vis–UV) spectrophotometer. PL and PL excitation (PLE) spectra were recorded using a Shimazu PF-5300PC fluorescence spectrophotometer with a photomultiplier tube operating at 110 V, and a 150 W Xe lamp as the light source. The near-infrared PL was collected using fibre-coupled spectrometers (NIRQUESTQ512, Ocean Optics), with laser diodes under excitation at λ = 405 nm and λ = 473 nm. PL decay at λ = 617 nm was measured by using a time-correlated single-photon-counting module (Quantaurus-Tau, Hamamatsu Photonics) equipped with a pulsed flash lamp (temporal resolution of 0.5 μs) with a band pass filter (central λ = 405 nm and full width at half maximum of 10 nm). All the measurements were performed at room temperature.

3. Results and Discussion

Figure 1 shows the DTA curve of the as-made glass. A broad exothermic peak appears at approximately 357–524 °C, representing the crystallisation temperature of Ag nanoparticles. When the sample was gradually heated, an obvious endothermic peak appeared as the temperature was above 530 °C, which was followed by an exothermic peak. The glass remained a good transparency after the heat treatment at 550 °C. No other crystals were found in the glass besides Ag nanoparticles. Figure 2 (a) shows a TEM image of the as-made glass. Only a few nanoparticles of diameter 2–3 nm exist in the glass matrix, which explains the absence of SPR absorption peak in this sample. The lattice structure of an individual Ag nanoparticle is revealed by the enlarged image shown in the inset of Fig. 2 (a). Figure 2 (b) shows the TEM image for HT500, demonstrating many Ag nanoparticles with the mean size of 4–5 nm. Compared with the as-made glass, both the concentration and diameter of Ag nanoparticles are increased by the heat treatment at 500 °C.

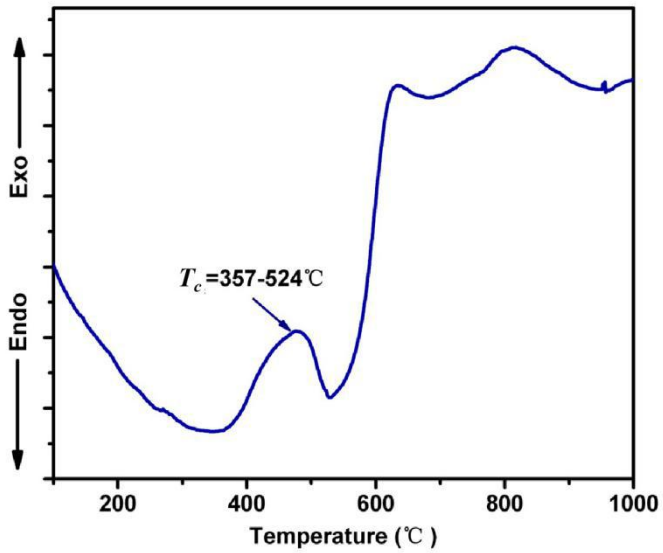

Figure 1 DTA curve of the $65B_2O_3$-$27Na_2CO_3$-$8Al_2O_3$-$0.2Sm_2O_3$-$1AgNO_3$ glass sample.

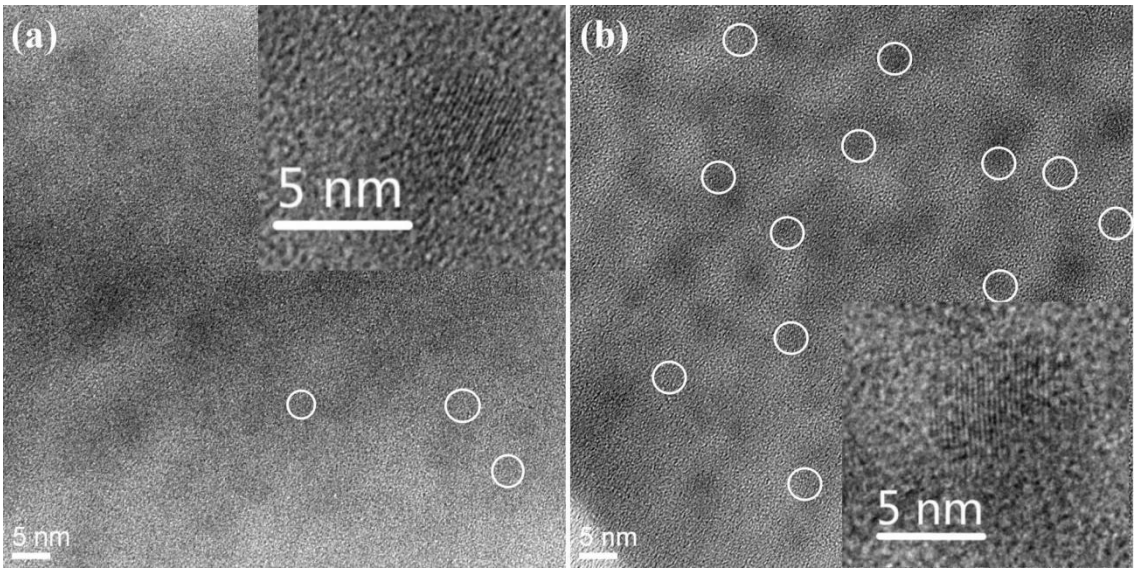

Figure 2 (a) TEM images of the (a) as-made glass and (b) HT500. The circles indicate the positions where the lattice patterns of Ag are recognised. The insets in (a) and (b) show the enlarged images of the as-made glass and HT500, respectively.

Figure 3 shows the NIR–Vis–UV absorption spectrum for the as-made glass and heat-treated samples. The sharp absorption peak at λ= 400 nm corresponds to the $^6H_{7/2}\rightarrow{}^4G_{5/2}$ transition of Sm^{3+}. In contrast to the as-made glass, with the increase in heat-treatment temperature, there is an emerging broad absorption peak in the range λ = 370–550 nm in the spectra, attributed to the SPR of Ag nanoparticles [35]. The SPR peak is not observed for the as-made glass in spite of the presence of Ag nanoparticles in the TEM image, because of the small number density of the nanoparticles. For the samples heat-treated from 350 to 500 °C, the increase in SPR absorption near λ = 425 nm is due to the increase in the particle number and size of Ag nanoparticles. When

the temperature reaches 550 °C, the SPR absorption peak becomes slightly red-shifted and broadened and the intensity decreases. This is probably because the larger nanoparticles migrate and merge into even larger particles whereas the smaller nanoparticles start to dissolve as the heat-treatment temperature approaches the melting temperature of Ag (=961 °C).

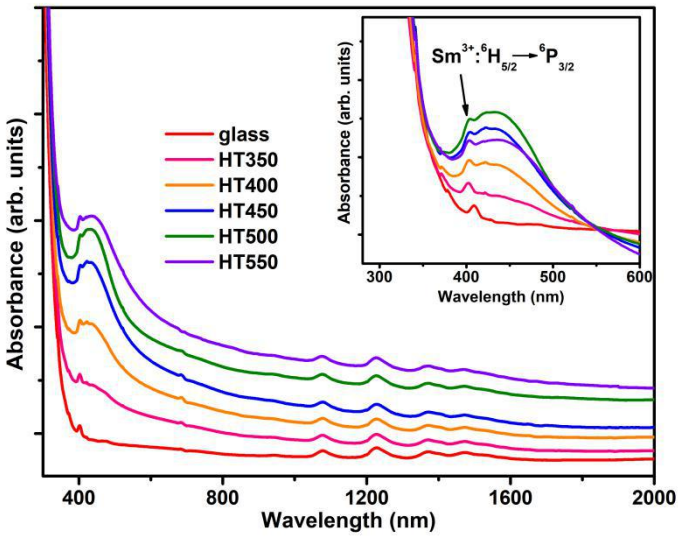

Figure 3 Absorption spectra of the as-made glass and the heat-treated samples. The spectra were shifted vertically for the sake of clarity. The inset shows the normalised absorption spectrum of each sample.

We measured the excitation spectra by monitoring light of λ = 600 nm for the as-made glass and heat-treated samples as shown in Figure 4 (a). The monitoring wavelength λ = 600 nm corresponds to the $^4G_{5/2}\rightarrow{}^6H_{7/2}$ transition for Sm^{3+}. All the samples have six peaks, at λ = 316, 343, 360, 375, 400, and 470 nm, corresponding to $^6H_{5/2}\rightarrow{}^4P_{3/2}$, $^4D_{7/2}$, $^4D_{3/2}$, $^6P_{7/2}$, $^6P_{3/2}$, and $^4M_{15/2}$ transitions, respectively [36,37]. Notably, with the increase in the SPR absorption from the as-made glass to HT500, the excitation spectrum reaches the maximum peak intensity. This is due to the enhanced probability of the electron transition of Sm^{3+} from the ground state $^6H_{7/2}$ to the excited state owing to the intensified electric field near the Ag nanoparticles [38]. According to the selection rule, the transition probability is proportional to the square of the absolute value of dipole moment [39,40]. The optimal excitation wavelength for the $^6H_{7/2}\rightarrow{}^4G_{5/2}$ transition of Sm^{3+} is λ = 400 nm, and the broadband SPR absorption peaks are in the range λ = 360–550 nm with the local maximum at λ = 425±20 nm. This indicates that the same wavelength that excites Sm^{3+} also stimulates the SPR effect of Ag nanoparticles in glass. In HT550, however, the SPR peak is apparently red-shifted. This shift leads to a mismatch between the spectral positions of Sm^{3+} transition and SPR and weakens the coupling effect. The spectral shape of PL excitation does not

vary whereas the intensity changes with the heat-treatment temperature, indicating the absence of an energy transfer effect from Ag^{+} to rare-earth ions, which has been reported in other glass systems [41, 42].

Figure 4 (b) shows the visible PL spectra of Sm^{3+} under excitation at λ = 400 nm for the as-made glass and heat-treated samples. The PL peaks at λ = 565, 600, and 640 nm correspond to the $^{4}G_{5/2}\rightarrow{}^{6}H_{5/2}$, $^{6}H_{7/2}$, and $^{6}H_{9/2}$ transitions of Sm^{3+}, respectively. As shown in the figure, the PL of Sm^{3+} in the region λ = 500–700 nm is enhanced, and for HT500, the intensity increases up to 39.8%. However, the PL of Sm^{3+} is significantly reduced for HT550, in accordance with that observed for the excitation spectra in Fig. 4(a).

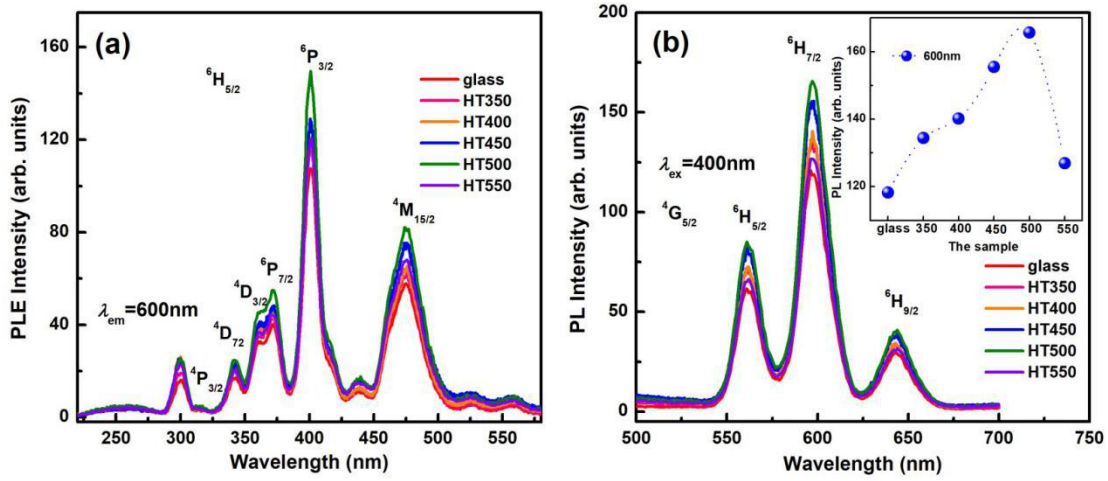

Figure 4 (a) Excitation spectra monitored at λ = 600 nm and (b) PL spectra of the as-made glass and heat-treated samples under excitation at λ = 400 nm. The inset in (b) plots the peak intensity at λ = 600 nm.

Figure 5 shows the near-infrared PL spectra (λ = 800–1700 nm) for the as-made glass and HT500 under excitation at λ = 405 nm. Sm^{3+} shows three distinct infrared PL peaks in the range λ =800–1700 nm: λ = 950 nm ($^{4}G_{5/2}\rightarrow{}^{6}F_{3/2}$, $^{6}F_{5/2}$), 1196 nm ($^{4}G_{5/2}\rightarrow{}^{6}F_{9/2}$), and 1290 nm ($^{6}F_{5/2}\rightarrow{}^{6}H_{5/2}$). Among them, the transition at λ = 950 nm is most useful for Si solar cell applications. By comparison, it can be observed that the infrared PL of Sm^{3+} from the HT500 is stronger than that of the as-made glass, and the integral intensities of PL peaks are enhanced by 25% (λ = 950 nm), 29% (λ = 1196 nm), and 28% (λ =1290 nm). The reason for the enhancement of the PL of Sm^{3+} in the near-infrared region is the same as that in the visible region, i.e. the near-infrared PL is also derived from the radiative transition from $^{4}G_{5/2}$. In addition, under excitation at λ = 473 nm, the PL of Sm^{3+} is increased by 55.5% (λ = 950 nm), 50% (λ = 1193 nm), and 52% (λ = 1289 nm) as shown in Figure 6. In the near-infrared region, the PL under excitation

at λ = 473 nm is stronger than that at λ = 400 nm. The reason may be that, under excitation at λ = 473 nm, the electrons transit from the ground state $^6H_{5/2}$ to the excited state of $^4M_{15/2}$ and thereafter the relaxation transition state of $^4G_{5/2}$, whereas under excitation at λ = 400 nm, electrons undergo relaxation from $^6P_{3/2}$ to $^4G_{5/2}$, which has a greater energy level difference. Owing to the larger relaxation energy before radiative transition, excitation at λ = 400 nm suffers from greater energy transfer to Ag nanoparticles, resulting in a smaller enhancement.

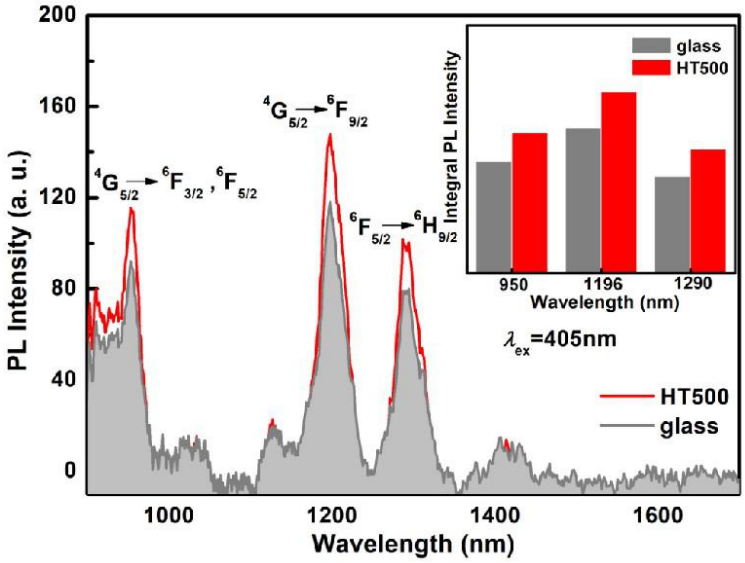

Figure 5 Near-infrared PL spectra of the as-made glass and HT500 under diode laser excitation at λ = 405 nm. The inset shows the integral intensities of near-infrared PL peaks.

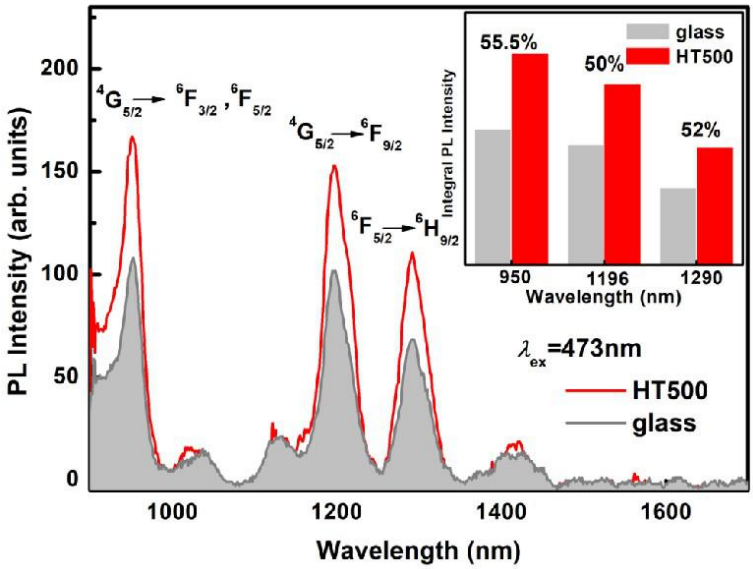

Figure 6 Near-infrared PL spectra of the as-made glass and HT500 under diode laser excitation at λ = 473 nm. The inset shows the integral intensities of near-infrared PL peaks.

We monitored the PL lifetimes of the transition of $^4G_{5/2}$ to $^6H_{7/2}$ (at λ = 600 nm) of Sm^{3+} using a pump of wavelength λ = 400 nm. Figure 7 (a) shows the PL lifetime of the as-made glass and

HT500. The decay of HT500 is faster than that of the as-made glass. The small component at the beginning of the decay corresponds to instrumental stray light from the excitation pulse. The PL decay curves were fitted by a single exponential function to obtain the PL lifetime τ of Sm^{3+} of 3.06 and 2.93 ms for the as-made glass and HT500, respectively. The inset of Fig. 7 (a) shows the decay curve of the Sm^{3+}-doped as-made glass prepared in the absence of $AgNO_3$, which also exhibits single exponential behaviour. Figure 7 (b) summarises the values of τ obtained from the fits. For the as-made glass, τ is similar to that of the Sm^{3+} singly-doped glass, which indicates that the PL lifetime is not affected by Ag^{+}. In the presence of Ag nanoparticles, τ decreases gradually until it reaches a minimum for HT500. The decrease in PL lifetime could indicate an increase in radiative or nonradiative decay rates. Here, the spectral position of SPR is shorter than that of PL and thus, we speculated that a change in radiative decay did not occur. We attributed it to an increase in the nonradiative energy transfer to Ag nanoparticles, and calculated the energy transfer efficiency (η_{ET}) as a ratio of k_{ET} ($=1/\tau-1/\tau_0$) to the total decay rate $1/\tau$ as follows:

$$\eta_{ET} = 1 - \tau / \tau_0 \qquad (1)$$

where τ_0 represents the PL lifetime of Sm^{3+} singly-doped glass. The energy transfer to Ag nanoparticles reduces the PL intensity. After heat treatment at 500 ºC, the reduction of τ is most apparent, showing an energy transfer efficiency of η_{ET} = 4.56%. The increase in PL intensity observed for HT500 indicates that the effect of excitation enhancement outweighs the negative effect of energy transfer.

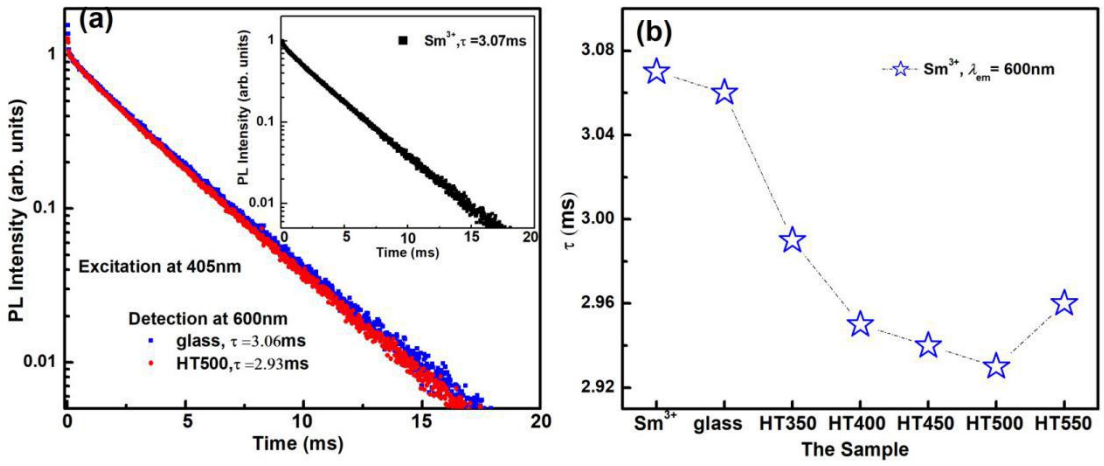

Figure 7 (a) PL decay curves monitored at λ = 600 nm (Sm^{3+}: $^4G_{5/2} \rightarrow {}^6H_{7/2}$) under the excitation at λ = 400 nm for the as-made glass and HT500. The inset shows the decay curve for Sm^{3+}-doped as-made glass in the absence of Ag. (b) PL lifetimes calculated from the single exponential fit to the experimental curves.

Figure 8 illustrates the energy levels of Sm^{3+} and SPR, together with the absorption, excitation, and PL spectra of the sample. For the visible PL under excitation at λ = 400 nm, electrons transit from the ground state $^6H_{5/2}$ to the excited state of $^6P_{3/2}$, and thereafter to the light-emitting $^4G_{5/2}$ level through multi-phonon relaxation. Finally, characteristic visible light is emitted in the transition to $^6H_{5/2}$, $^6H_{7/2}$, and $^6H_{9/2}$ levels. For the near-infrared PL, the excited electrons in $^4G_{5/2}$ level radiatively transit to $^6F_{3/2}$, $^6F_{5/2}$, $^6F_{9/2}$, and $^6F_{5/2}\rightarrow{}^6H_{5/2}$ to emit the characteristic near-infrared light [43-45]. There is a significant overlap between the SPR peak and the excitation spectrum. Under irradiation with light of λ = 400 nm (405 nm and 473 nm in the case of near-infrared PL measurements), Ag nanoparticles in the glass strongly couple with the incident light to generate a strong localized electromagnetic field via the excitation of SPR. This increases the transition probability of the electrons of Sm^{3+} to the excited levels and enhances the visible and near-infrared PL.

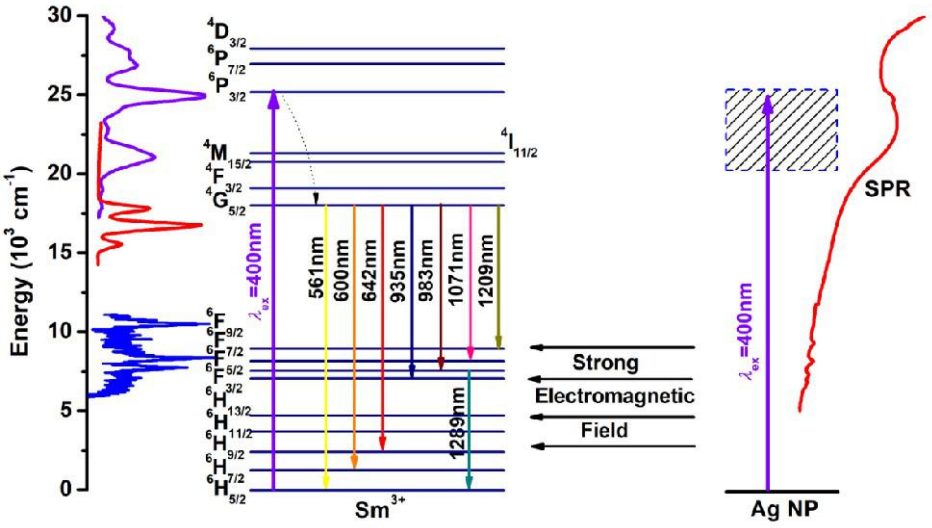

Figure 8 (Left) PL and PL excitation spectra of the sample, (centre) the energy diagram of Sm^{3+}, (right) SPR spectrum of the sample and the energy diagram for Ag SPR.

In order to further analyze the SPR effect on the enhancement of Sm^{3+} PL, we compare the PL excitation, PL spectra, SPR absorption intensity, and SPR spectral position of the samples. Figure 9 (a) shows the cross-sectional areas of SPR absorption at approximately λ = 420 nm for the samples. Compared with the as-made glass, the heat-treated samples showed increased cross-sectional areas of absorption, which reach a maximum value for HT500 and thereafter decrease for HT550. Figure 9 (b) shows the central position of the SPR absorption peak. There is a red shift with the increase in heat-treatment temperature. Figures 9 (c) and (d) show the PL

intensity and excitation plots for the samples at λ = 600 nm and 400 nm, respectively. We can observe a correspondence between the SPR absorption intensity and the PL intensity. Following the increase in the cross-sectional area of SPR, both the PL and PLE of Sm^{3+} are enhanced. The correlation suggests the absence of Ag-related optical centres such as Ag^{+} clusters, i.e. the choice of aluminoborate glass as a matrix allows for the elucidation of the effect of SPR on the PL of Sm^{3+}.

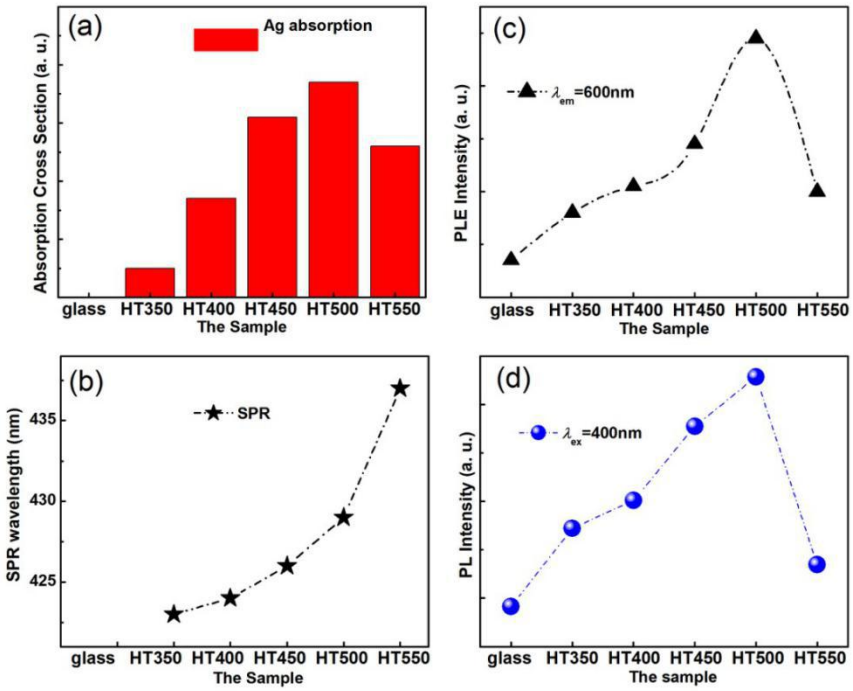

Figure 9 (a) Absorption cross-section and (b) centre of SPR peaks for the as-made glass and the heat-treated samples. (c) and (d) are PLE and PL intensity plots for the samples monitored at λ = 600 nm and excited at λ = 400 nm, respectively.

4. Conclusion

Aluminoborate glasses containing Ag^{+} and Sm^{3+} were prepared via a melt-quenching method. After the heat treatment, Ag became aggregated as nanoparticles in the glass. The Ag nanoparticles coupled with the excitation light through the strong localized electromagnetic field accompanying SPR. This enhancement under the excitation process led to a net increase in PL intensity, although the measurement of PL lifetime indicated a slight energy transfer to Ag nanoparticles, which acted as a nonradiative path. The PL enhancement was correlated to the SPR strength in absorption spectra, confirming that the excitation enhancement by the SPR was the origin of PL enhancement. For the samples heat-treated at 500 °C, the strengths of visible (λ = 600 nm) and near-infrared (λ = 950 nm) PLs of Sm^{3+} reached the maximum values of 39.8% and 25%, respectively, of that of the as-made glass. By utilizing the effect of SPR on Sm^{3+}, the heat-treated

glass presented herein may be beneficial for the improvement of polycrystalline Si photoelectric conversion efficiency.

Acknowledgements

The authors thank the nanotechnology platform for the TEM observation. A part of this work was supported by the Kyoto University Nano Technology Hub Nanofabrication Platform in 'Nanotechnology Platform Project' sponsored by the Ministry of Education, Culture, Sports, Science and Technology (MEXT), Japan. YG gratefully acknowledges support from the JSPS Fellowship (No. 18J14889). Financial support from Grant-in-Aid for Scientific Research (B, No.16H04217) by MEXT is acknowledged.

Reference

[1] G. D. Scholes, G. R. Fleming, A. Olaya-Castro. Nature Chem. 3 (2011) 763-774.

[2] A. Yella, H. W. Lee, H. N. Tsao. science 334 (2011) 629-634.

[3] X. Wang, G. I. Koleilat, J. Tang. Nature Photo. 5 (2011) 480-484.

[4] W. Shockley, H. J. Queisser, J. Appl. Phys. 32 (1961) 510-519.

[5] T. Trupke, A. Shalav, B. S. Richards. Sol. Energ. Mat. Sol. C. 90 (2006) 3327-3338.

[6] G. F. Brown, J.Wu, Laser Photonics Rev. 3 (2009) 394-405.

[7] D. M. Powell, M. T. Winkler, H. J. Choi. Energ. Environ. Sci. 5 (2012) 5874-5883.

[8] M. A. Green, K. Emery, Y. Hishikawa. Prog. photovoltaics: research and applications, 23 (2015) 1-9.

[9] L. L. Li, E. W. Diau. Chem. Soc. Rev. 42 (2013) 291-304.

[10] Z. Hosseini, N. Taghavinia, E. W. Diau. ChemPhysChem 18 (2017) 3292-3308.

[11] J. H. Wu, J. L Wang, J. M. Lin. Sic. Rep. 3 :2058 |DOI:10.1038/srep02058.

[12] X. Jin, H. Y. Li, D. Y. Li. Opt. Express 24 (2016) A1276-A1287.

[13] G. M. Akselrod, C. Argyropoulos, T. B. Hoang. Nature Photo. 8 (2014) 835-840.

[14] J. M. McLellan, Z. Y. Li, A. R. Siekkinen. Nano lett. 7 (2007) 1013-1017.

[15] F. Omnes, J. C. Guillaume, G. Nataf. IEEE T. Electron Dev. 1996, 43(11): 1806-1811.

[16] R. J. Amjad, M. R. Sahar, M. R. Dousti. Opt. express 21 (2013) 14282-14290.

[17] N. Shasmal, K. Pradeep, B. Karmakar. RSC Adv. 5 (2015) 81123-81133.

[18] T. Hayakawa, S.T. Selvan, M. Nogami. J. Non-cryst. Solids. 259 (1999) 16-22.

[19] D. Rajesh, M. R. Dousti, R. J. Amjad. J. Lumin. 192 (2017) 250-255.

[20] G. Okada, B. Morrell, C. Koughia, A. Edgar, C. Varoy, G. Belev, T. Wysokinski, D. Chapman, S. Kasap. Appl. Phys. Lett. 99 (2011) 121105.

[21] T. Som and B. Karmakar. J. Mod. Opt. 58 (2011) 1012-1023.

[22] I. Mechergui, H. fares, S. A. Mohamed, M. Nalin, H. Elhouichet. J. lumin. 190 (2017) 518-524.

[23] N. M. Yusoff, M. R. Sahar. Mater. Sci. Forum. 846 (2016) 107-114.

[24] L. Bolundut, E. Culea, G. Borodi, R. Stefan, C. Munteanu, P. Pascuta. Int. Ceram. 41 (2015) 2931-2939.

[25] M. R. Dousti, R. J. Amjad, R. Hosseinian, M. Salehi, M. R. Sahar. J. Lumin. 159 (2015) 100-104.

[26] J. A. Jimenez, M. Sendova. Solid State Commun. 152 (2012) 1786-1790.

[27] S. Thomas, M. S. Sajna, K. N. Rasool, M. Gopinath, C. Joseph, N. V. Unnikishnan. Opt. Mater. 39 (2015) 167-172.

[28] A. Herrera, S. Buchner, R. V. Camerini, C. Jacinto, N. M. Balzaertti. Opt. Mater. 52 (2016) 230-236.

[29] Z. Guo, S. Ye, T. Liu, S. Li, D. Wang. J. Non-cryst. Solids 458 (2017) 80-85.

[30] T. Som, B. Karmakar. Spectrochim. Acta A: Molecular and Biomolecular Spectroscopy, 75 (2010) 640-646.

[31] N. Shasmal, K. Pradeep, B. Karmakar. RSC Adv. 5 (2015) 81123-81133.

[32] L. J. Li, Y. Yang, D. C. Zhou, Z. Yang, X. Xu, J. Qiu. J. Appl. Phys. 113 (2013) 193103.

[33] Q. Jiao, X. Yu, X. H. Xu. J. Appl. Phys. 114 (2013) 043107.

[34] S. Thomas, M. Sajna, S. N. Rasool. Opt. Mater. 39 (2015) 167-172

[35] L. Li, Y. Yang, D. Zhou. J. Appl. Phys. 113 (2013) 193103.

[36] Evanoff, D. David, C. George, ChemPhysChem 6 (2005) 1221-1231.

[37] H. Lin, E. Y. B. Pun, L. H. Huang. Appl. phys. lett. 80 (2002) 2642-2644.

[38] A. Herrmann, M. Tylkowski, C. Bocker. J. Mater. Sci. 48 (2013) 6262-6268.

[39] U. Kreibig, C. Fragstein. Z. Phys. A: Hadrons Nucl. 224 (1969) 307-323.

[40] S. Murai, M. Saito, H. Sakamoto. APL Photo. 2 (2017) 026104.

[41] J. J. Li, R. F. Wei, X. Y. Liu, H. Guo. Opt. Express 20 (2012) 10122-10127.

[42] D. Rajesh, R. J. Amjad, M. R. Dousti, A. S. S. de Camargo. J. Alloy. Compd. 695 (2017) 607-612.

[43] F. Jing, S. Harako, S. Komuro. J. Phys. D: Appl. Phys. 42 (2009) 085109.

[44] J. J. Velázquez, V. K. Tikhomirov, L. F. Chibotaru. Opt. express 20 (2012) 13582-13591.

[45] W. Luo, R. Li, X. Chen. J. Phys. Chem. C 113 (2009) 8772-8777.